ELSEVIER

Polymer 42 (2001) 5257–5266

polymer

www.elsevier.nl/locate/polymer

# Investigation of secondary crystallization of polymers by means of microbeam X-ray scattering

R. Kolb[a,*], C. Wutz[b], N. Stribeck[b], G. von Krosigk[b], C. Riekel[c]

[a] *ExxonMobil Research and Engineering Company, Route 22 East, Annandale, NJ 08801 USA*
[b] *Institut fuer Technische und Makromolekulare Chemie, University of Hamburg, Hamburg, Germany*
[c] *European Synchrotron Radiation Facility, Grenoble, France*

This paper is dedicated to the memory of Prof. Dr H.G. Zachmann

Received 15 June 2000; received in revised form 27 November 2000; accepted 27 November 2000

**Abstract**

The kinetics of secondary crystallization during spherulite growth of isotactic poly(propylene) (iPP) and poly(vinylidene flouride) ($PVF_2$) is studied using a novel technique that employs a micron size X-ray beam. The data are combined with separate conventional simultaneous on-line SAXS/WAXS measurements and optical microscopy studies. In our experiments, crystallization takes place at low undercooling so that slowly growing large single spherulites are obtained. The data reveal that the main mechanism of secondary crystallization is the growth of new lamellae stacks within remaining amorphous regions. It is shown that a substantial amount of crystallites form as a result of secondary crystallization while the spherulite is growing. Furthermore, secondary crystallization is strongest directly behind the boundary of the spherulite and is independent of its size or growth state. A separate, off-line microfocus study on a quenched spherulite sample confirms this observation; the crystallinity is higher in the main body of the spherulite and lower near the boundary, where crystallization progressed to a lesser degree. 

*Keywords*: Crystallization kinetics; Spherulite; Microbeam X-ray Scattering

## 1. Introduction

During isothermal crystallization of polymers from the quiescent melt, one often observes the formation and growth of spherulites or other morphological entities. A spherulite consists of crystal lamellae and noncrystalline regions; thus, the *crystallinity* within these morphological units is usually far less than 100%. The first step of the crystallization process, when the spherulites grow until they impinge on each other is denoted as *primary crystallization*. A *secondary crystallization* process can be observed when the sample is completely composed of spherulites. At this time, an increase in crystallinity can only occur within the spherulitic macrostructure [1]. In principle, secondary crystallization can involve thickening of the crystals, growth of new lamellae within or between existing lamellae stacks, and growth of entire new lamellae stacks from remaining amorphous regions within the spherulites. A refinement of existing crystals through the removal of lattice defect distortions is also possible.

Often, Avrami's theory is used to interpret the sigmoidal shape of the crystallization curve [2]. The theory, however, assumes that the crystallinity within the growing entities is constant during spherulite growth and unsuccessfully describes the later state of primary crystallization. Therefore, the Avrami equation has been modified to account for secondary crystallization [3–5].

The nature of secondary crystallization was studied in a number of real time experiments and scattering methods, such as small- and wide-angle X-ray scattering (SAXS and WAXS), and light scattering (LS) were widely used [6–10]. Sometimes these methods were combined with differential scanning calorimetry (DSC) [11,12]. Schultz et al. performed simultaneous measurements of SAXS/WAXS/LS and found lamellar thickening, growth of new crystals within existing lamellae stacks, and formation of new lamellae to occur. The authors assumed that the crystallinity was constant within the spherulite during its growth and that Avrami's theory could be applied [7]. Wang et al. investigated the secondary crystallization of Poly(ethylene terephthalate) [13]. They used a correlation function method to extract the lamellar thickness from the SAXS data. To explain their results, Wang et al. favored a lamellar insertion

* Corresponding author. Tel.: +1-908-730-2970; fax: +1-908-730-3314.
*E-mail address:* rkolb@erenj.com (R. Kolb).

0032-3861/01/$ - see front matter 
PII: S0032-3861(00)00920-4

model as the most important mechanism during secondary crystallization of PET. Further progress has been made by Akpalu et al., who performed simultaneous SAXS/WAXS, and independent LS and DSC studies on polyethylene [14]. The authors were able to separate secondary and primary crystallization effects at the end of the spherulite growth period. It was concluded that secondary crystallization was predominant at the end of spherulite growth.

The present paper introduces a new method to study secondary crystallization during spherulite growth employing microbeam wide-angle X-ray scattering (μWAXS). A micron size X-ray beam was used to monitor the structural changes inside the spherulite while it was growing. Two polymers that form sufficiently large spherulites, namely isotactic poly(propylene) (iPP) and poly(vinylidene fluoride) ($PVF_2$) were investigated. To supplement the information about secondary crystallization, the microbeam data were combined with additional conventional on-line SAXS/WAXS measurements.

## 2. Experimental

### 2.1. General procedure

In order to study crystallization effects inside the growing spherulite most effectively, it was desired to study the kinetics of long periods during spherulite growth. Therefore, the polymers were crystallized at a temperature close to their melting point. Conventional time resolved measurements of SAXS/WAXS during isothermal crystallization were conducted to study the secondary crystallization processes after the spherulites had become volume filling. The experimental set up for the conventional SAXS/WAXS measurements during crystallization was described earlier by Zachmann et al. [8,11,12,15]. Further examples can be found by Ryan and Hsiao [13,16,17]. The wide- and the small-angle scattering were recorded simultaneously during isothermal crystallization of the polymer. This method employed a rather large focus covering an area of $2 \times 3\ mm^2$, which was far bigger than the spherulites yielding an average scattering curve of spherulites and the nonspherulitic regions. Here, this type of experiments is denoted as the *conventional method* to study the crystallization kinetics in order to distinguish it from the microfocus experiments described next.

The concept of the time resolved microfocus measurements made use of a very small focus that covered an arbitrary area of the sample, which was far smaller than the spherulites. The X-ray scattering of this area was recorded on-line by means of a two dimensional detector. The sample was molten and than cooled down to a crystallization temperature close to the melting point. Due to the low nucleation density at this temperature, very few spherulites grew at a slow rate and formed relatively large units. During the course of primary crystallization, one of them eventually grew over the area covered by the static X-ray focus. From this point of time, the changes in the X-ray pattern were due to a secondary crystallization process *inside* of the growing spherulite. The use of very thin specimens having a thickness of about 10 μm ensured that only one spherulite is observed by the microbeam. A schematic sketch of the experimental conception is shown in Fig. 1. Experiments in which crystallization within the spherulite was observed early during its growth were especially significant, because a longer period of secondary crystallization during spherulite growth could be studied.

Since it could not be controlled at which growth state the spherulite will cross the area covered by the X-ray focus, the experiments had to be repeated many times. This way, the beginning of the secondary crystallization process was randomly captured at different stages of spherulite growth. In the case of iPP eight experiments and in the case of $PVF_2$ seven experiments were performed. In order to control if the microfocus experiments indeed took place *during* spherulite growth, they were compared with the corresponding conventional measurements and optical microscopy studies.

As we study secondary crystallization during spherulite growth, it might be useful to redefine secondary crystallization at this point: "secondary crystallization takes place in a confined environment from the noncrystalline regions in the presence of existing crystals, whereas primary

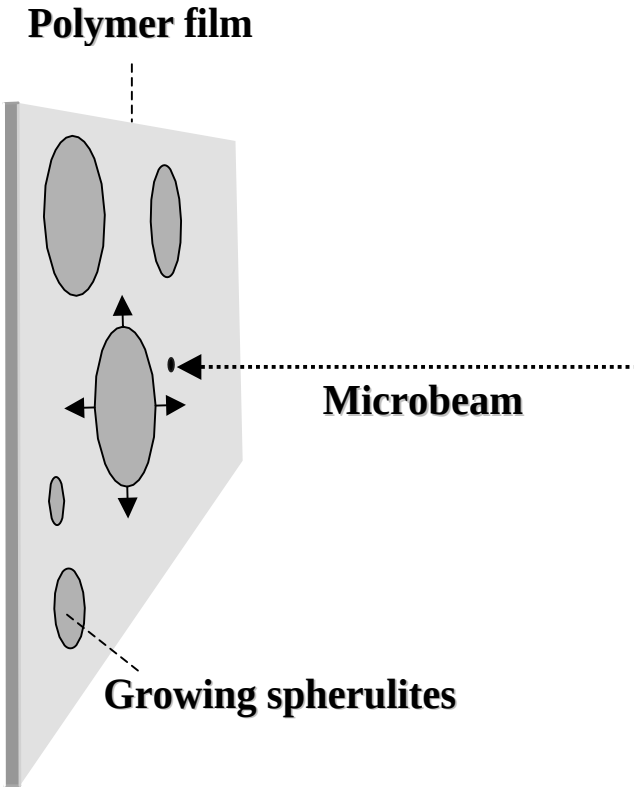


Fig. 1. Schematic sketch of the conception for the microfocus experiments to study secondary crystallization inside a growing spherulite.

crystallization is crystallization from the free melt". This alternate definition was promoted earlier by Hsiao and Marand [18,19].

### 2.2. Material

Isotactic poly(propylene) (iPP) and poly(vinylidene flouride) ($PVF_2$) were used for this study. The iPP was supplied by Polyscience, Germany. It had a molecular weight, $M_w$, of 135,000 g/mol, and a melting temperature, $T_m$, of 162°C. The $PVF_2$ by Solvay, Germany had a $M_w$ of 80,000 g/mol, the melting temperature was 185°C. Both polymers did not contain any nucleating agents.

The conventional measurements of X-ray scattering during isothermal crystallization were performed on compression molded sheets of these materials having a thickness of about 100 μm. For the microbeam experiments, thin films of 10 μm thickness were prepared. The compression molding was done under vacuum 30°C above the melting temperature of the polymer.

### 2.3. Synchrotron facilities

The microbeam experiments were conducted at the undulator based microfocus beamline, BL1, at the European Synchrotron Radiation Facility (ESRF) in Grenoble, France. The white synchrotron beam was monochromatized by reflection from a channel cut Si (111) monochromator resulting in a wavelength of 0.09 nm. A rhodium coated ellipsoidal mirror was employed to focus the beam to a size of $10 \times 10\ \mu m^2$. To further decrease the spot size, glass capillary optics were used enabling a focus of $2 \times 2\ \mu m^2$ to be achieved. A detailed description of the beamline can be found by Engstrom, Fiedler, and Riekel [20]. A two-dimensional CCD detector by Micro Photonics was used to record the wide-angle X-ray patterns. The detector was placed at a distance of 11 cm from the sample. The accumulation time was 15 s per picture.

The conventional measurements of SAXS and WAXS during isothermal crystallization were performed at the polymer beamline, A2, at the Hamburg Synchrotron Radiation Laboratory (HASYLAB) at the German Electron Synchrotron, DESY, in Hamburg, Germany. The energy of the radiation was 8 keV. Further information of the beamline can be found elsewhere [21]. To record the WAXS and the SAXS curves, one-dimensional proportional counters were used. These counters were placed at distances of 12 cm (WAXS) and 2200 cm (SAXS) from the sample. The accumulation time was 20 s per frame. In order to protect the specimen from degradation, the thermal treatment of the specimens took place in a vacuum chamber.

### 2.4. Optical microscopy

To measure the radial growth rates of the spherulites, the material was molten between glass plates and isothermally crystallized at different temperatures using a Linkam hot stage. The sample was placed between crossed polarizers and the spherulite growth was observed through a microscope and measured by means of a micrometer scale and a stopwatch.

### 2.5. X-ray scattering

Prior to analyzing, the data were normalized for the intensity of the primary beam. Furthermore, corrections for an electronic background of the detector, and the background scattering were applied. Two-dimensional X-ray patterns obtained during the microfocus experiments were used to determine the crystallinity, $x_c$. $x_c$ was calculated from an averaged scattering curve by fitting an amorphous halo. The amorphous halo was obtained from the molten sample. For anisotropic scattering patterns exhibiting a rotational symmetry, $x_c$ can be approximated by

$$x_c = \frac{\int_0^{\pi}\int_{s_0}^{s_1} I_C(s,\vartheta)s^2 \sin\vartheta\, ds\, d\vartheta}{\int_0^{\pi}\int_{s_0}^{s_1} I(s,\vartheta)\, s^2 \sin\vartheta\, ds\, d\vartheta}, \quad (1)$$

where $I_C$ is the intensity of the crystal reflections and $I$ represents the scattering intensity of both the amorphous and the crystalline part, $\vartheta$ is the polar angle and $s = 2\sin\theta/\lambda$ the scattering vector. To calculate $x_c$, it was assumed that the orientation of the crystals did not change during the course of crystallization. Careful analysis of the two dimensional X-ray patterns proved that the orientation did indeed not change during the course of spherulite growth. In the case of the conventional WAXS measurements, where isotropic scattering curves were obtained, the equation simplifies to

$$x_c = \frac{\int_{s_0}^{s_1} I_C(s)s^2\, d^s}{\int_{s_0}^{s_1} I(s)s^2\, ds} \quad (2)$$

The relative small-angle invariant, $Q$, has been calculated from

$$Q = 4\pi \int_{s_0}^{s_1} I(s)s^2\, ds \quad (3)$$

after correction for background scattering, scattering volume, absorption, and decay of the primary beam. The long period, $L$, was determined from the maximum of the small-angle reflection after Lorentz correction.

## 3. Results and discussion

### 3.1. Optical microscopy

The spherulite sizes and growth rates for the two different polymers were determined by optical microscopy for various crystallization temperatures, $T_C$. Additionally, the

Table 1
Spherulite diameter, half time of primary crystallization, crystallization rate, and crystallization temperature for the different experimental conditions

| Polymer | Spherulite diameter (μm) | Half time of crystallization (min) | Crystallization rate (μm/min) | Crystallization temperature (°C) |
|---|---|---|---|---|
| *Poly(propylene)* | | | | |
| (a) Microscope measurement | 80 | 33 | 1.5 | 148 |
| (b) Conventional X-ray measurement | 84 | 34 | – | 148 |
| (c) Microfocus X-ray measurement | 83 | – | – | 148 |
| *Poly(vinylidene fluoride)* | | | | |
| (a) Microscope measurement | 50 | 25 | 1.3 | 162 |
| (b) Conventional X-ray measurement | 50 | 25.5 | – | 162 |
| (c) Microfocus X-ray measurement | 52 | – | – | 162 |

sizes of the spherulites were measured after both the conventional and the microfocus crystallization experiments.

At $T_C = 148$°C, the iPP spherulites grew at a constant rate of 1.5 μm/min until they impinged on each other. After 66 min, the entire sample was composed of spherulites having an average end diameter of about 80 μm. These conditions provided both sufficiently long periods of growth and adequately large single spherulites necessary to perform the microfocus experiments. $PVF_2$ was crystallized at $T_C = 162$°C and formed spherulites that had a diameter of 50 μm and grew at a rate of 1.3 μm/min. The temperature conditions for both the conventional and the microbeam crystallization experiments were chosen according to the data obtained by optical microscopy. The results concerning the crystallization experiments on iPP and $PVF_2$ at $T_C = 148$°C, and $T_C = 162$°C, respectively, are summarized in Table 1.

### 3.2. Simultaneous on-line measurements of SAXS and WAXS during isothermal crystallization of iPP and $PVF_2$ (conventional study of the crystallization kinetics)

An example of the development of the SAXS and the WAXS as a function of time during isothermal crystallization of iPP at 148°C is shown in Fig. 2(a) and (b). After an induction period of 12 min at *T*c, crystal reflections became visible. At the same time, a small-angle peak started to appear. The half time of crystallization, $\tau_{(1/2)}$, was 34 min and the average spherulite size of the fully crystallized sample was 84 μm.[1] These values were in good agreement with the data obtained from the separate microscopy study during crystallization under the same conditions. The crystallinity for each of the curves in 2 (a) was calculated according to Eq. (2). From the SAXS curves the invariant, $Q$, and the long period, $L$, were determined as described earlier in this paper. Fig. 3 shows $x_c$, $Q$ and $L$ as a function of crystallization time for this experiment (the scattering invariant was normalized so that after twice the half time $x_c$ and $Q$ had the same value). During primary crystallization, both $Q$ and $x_c$ showed a sigmoidal increase. After twice $\tau_{(1/2)}$, primary crystallization was finished. In the following time, $x_c$ increased due to secondary crystallization from 53 to 58% within 200 min. During this time, $Q$ remained nearly constant. As the small-angle scattering invariant is proportional to $x_c(1 - x_c)$, a decrease of $Q$ of about 2.5% was expected during the first 200 min of secondary crystallization. This slight experimental discrepancy can be explained with statistical and systematic errors of the measurements.[2]

The long period was constant after 40 min of crystallization, which corresponds to $\tau_{(1/2)}$. Therefore, it can be concluded that the most important mechanism of secondary crystallization was either the growth of new lamellae stacks (of same lamellae thickness) into remaining amorphous regions or that existing lamellae grew thicker at the expense of amorphous regions. Formation of thinner crystals between lamellae within existing stacks would have caused a decrease of $L$ and can, therefore, be excluded. Moreover, due to the high crystallization temperature thinner lamellae are unlikely to grow because of their lower melting point. It is to be noted, however, that insertion of new (thick) lamellae into significantly large gaps ($>2L$) within the lamellar stack is still possible as pointed out by Schultz [22].

From the wide-angle scattering curves the full width at half maximum, FWHM, for three reflections, the (110), (040) and the (130) was extracted. Careful examination showed that FWHM did not change during the entire crystallization process. Furthermore, the analysis showed no shift of the positions of the reflections. Although the widths

[1] The spherulite size was determined by optical microscopy after the crystallization experiment.

[2] Determination of $x_c$ according to Eq. (1) does not yield the absolute degree of crystallization. If the true volume fraction of the crystals were 46% at the beginning of secondary crystallization and 53% after 6 h, no change in $Q$ would have been observed.

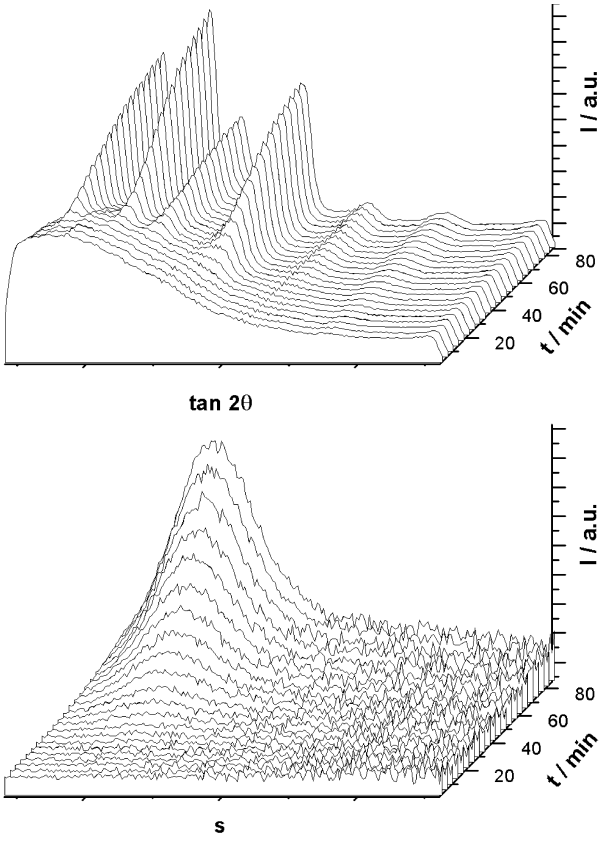


Fig. 2. Development of WAXS and SAXS during isothermal crystallization of iPP at 148°C: (a) WAXS, and (b) SAXS.

of the reflections are not very sensitive to small structural changes, it can be concluded that neither a substantial growth of the crystals nor a refinement of existing crystals occurred. These findings are not surprising since crystallization took place at low supercooling where growth occurred very slowly. Therefore, the resulting structures were relatively free of lattice defect distortion. Unfortunately, only (*hk*0) reflections were accessible and a determination of the lattice parameters of the c-axis (chain axis) was not possible.

In a second experiment, the isothermal crystallization of $PVF_2$ at $T_C = 162$°C was investigated. Fig. 4 shows the development of $x_c$, $Q$, and $L$ during isothermal crystallization of $PVF_2$ at $T_C = 162$°C as a function of time. The enlargement of the early part of the crystallization curves proves that SAXS appeared before crystal reflections could be detected. This indicates that SAXS, which detects electron density fluctuations, is more sensitive to structural changes at the beginning of crystallization than WAXS. This phenomenon can be easily observed in $PVF_2$ because of the large electron density contrast ($\rho_{amorph} = 1.67$ g/cm$^3$, $\rho_{crystalline} = 1.94$ g/cm$^3$). It will be discussed in great detail in a forthcoming paper [23].

The sample was crystallized for 180 min. After primary crystallization was finished (twice $\tau_{(1/2)}$), $x_c$ was 54%. During the following 130 min of secondary crystallization,

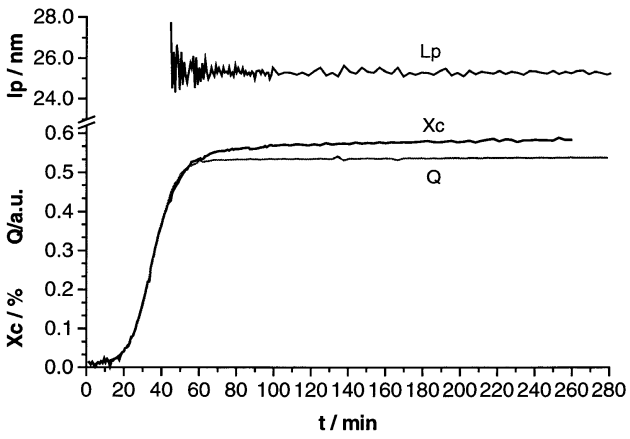


Fig. 3. Crystallinity, $x_c$, scattering invariant, $Q$, and the long period, $L$, as a function of crystallization for the isothermal crystallization of iPP at 148°C.

$x_c$ increased to 62%. $Q$ did practically not change. Analysis of the line widths of the wide-angle reflections showed no change of the lattice parameters. Similar to the experiments on iPP described above, $L$ was constant after 12 min of crystallization (just after a discrete SAXS signal could be detected), which can be explained by the low undercooling at which lamellae growth took place. From this it can be concluded that no thinner crystals grew between lamellae within existing stacks.

The conventional X-ray measurements of the crystallization kinetics demonstrated that both polymers investigated exhibited substantial secondary crystallization at constant $T_C$. After 220 min, or seven times $\tau_{(1/2)}$, 10% of the crystalline fraction of iPP was due to secondary crystallization. For $PVF_2$, $x_c$ increased by 13% as a result of secondary crystallization after seven times $\tau_{(1/2)}$.

At the present thermal condition (low undercooling), lamellae grew fairly slowly forming rather stable crystals close to their equilibrium size. Therefore, growth of new lamellae within remaining amorphous regions inside the spherulite was more likely to occur than a substantial lamellar thickening. Marand pointed out that at very low undercoolings there is a tendency for a more open and coarse structure of the lamellae to develop and new lamellae can grow from the relatively free melt. In this case the structural differences between primary and secondary lamellae should be very small [24]. The finding of a constant value of $L$ reported in this paper supports Marand's conclusion.

### *3.3. Microfocus measurements of WAXS during isothermal crystallization of iPP and $PVF_2$*

The thermal conditions for the microfocus measurements of secondary crystallization were the same as for the conventional kinetic measurements. Table 1 shows that the spherulites obtained during the microfocus measurements had the same diameter as the ones crystallized under the

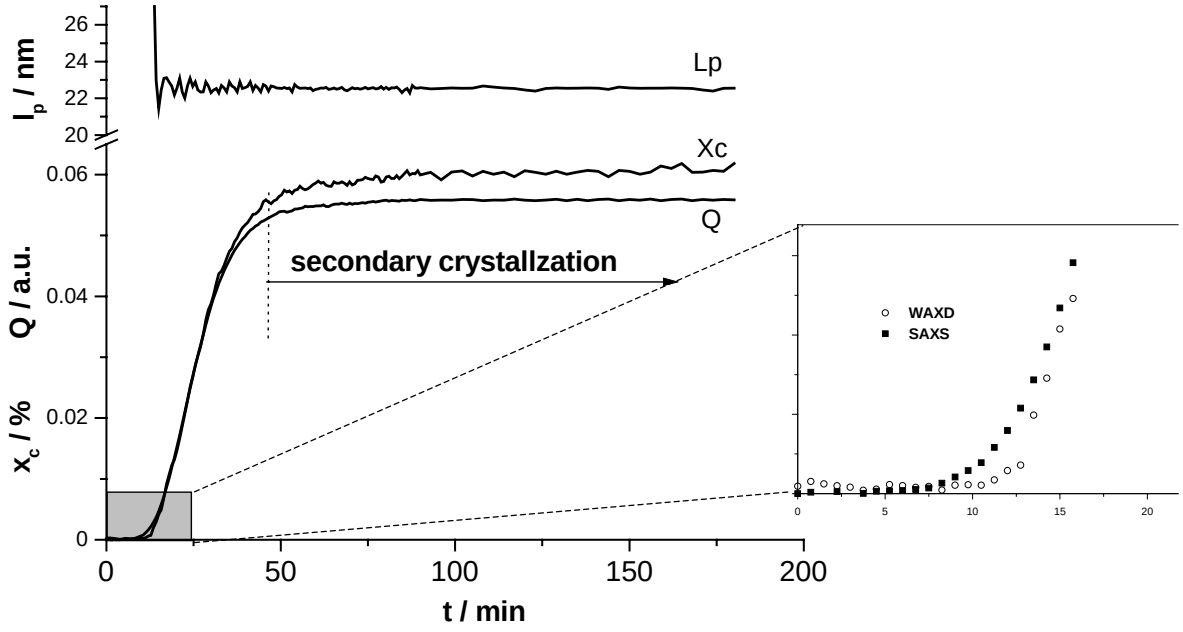


Fig. 4. Development of $x_c$, $Q$, and $L$ during isothermal crystallization of $PVF_2$ at $T_C = 162°C$ as a function of time. The scattering invariant was normalized. The enlargement shows the early part of the crystallization curves.

microscope. It is to be noted that the spherulite grew at a slower rate because of the small thickness of the films that were used during the microfocus experiments. After a three-dimensional beginning of the growth, the spherulites were forced into a two-dimensional geometry [25,26].

The development of the wide-angle scattering during the microfocus experiments is shown in Fig. 5(a) and (b) for the isothermal crystallization of iPP and PVF2, respectively. The initial scattering pattern showed no reflections, because the area covered by the microbeam was still amorphous

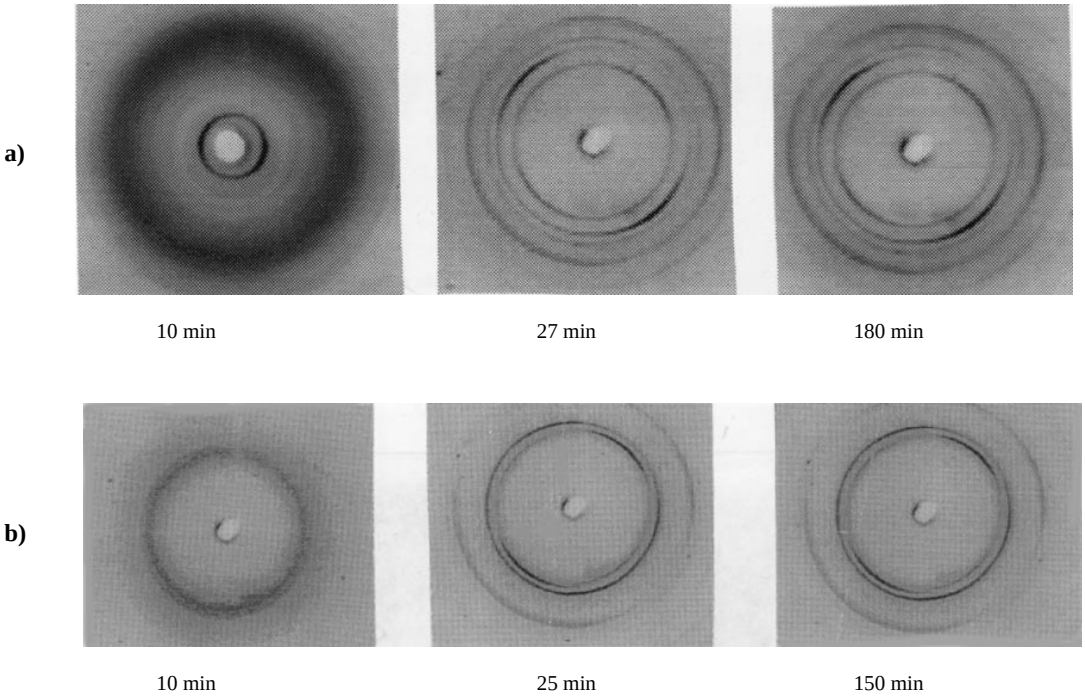


Fig. 5. Microfocus experiment: Development of WAXS during isothermal crystallization: three μWAXS patterns at different times during the crystallization of iPP: (a) and $PVF_2$, and (b) at $T_C = 148$ and 162°C, respectively, are shown. The left pictures show an amorphous scattering pattern, because no spherulite has crossed the irradiated area yet. The center and the right pictures are taken directly after the spherulite grew over the spherulite and at the end of the experiment, respectively. It is to be noted that the positions of the reflections do not change over the course of crystallization.

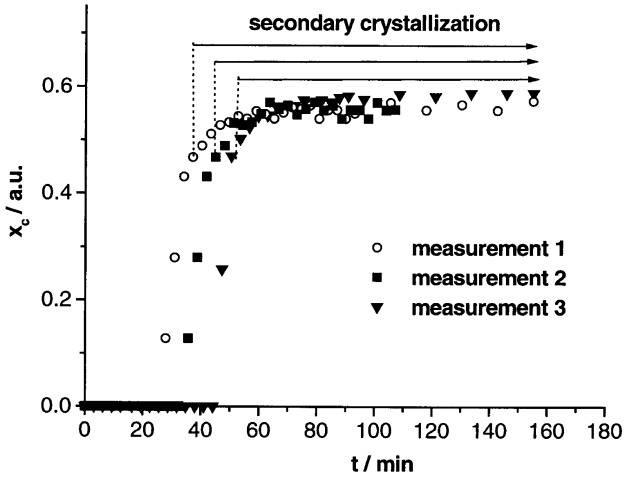


Fig. 6. $x_c$ as obtained from the microfocus experiments for the isothermal crystallization of iPP at 148°C. Data acquisition started when the sample had reached 148°C. The initial part of the curves shows no crystallization because the microfocus area has not yet been crossed by a growing spherulite. After the microfocus was completely in the spherulite, secondary crystallization is observed. A vertical line indicates this point of time.

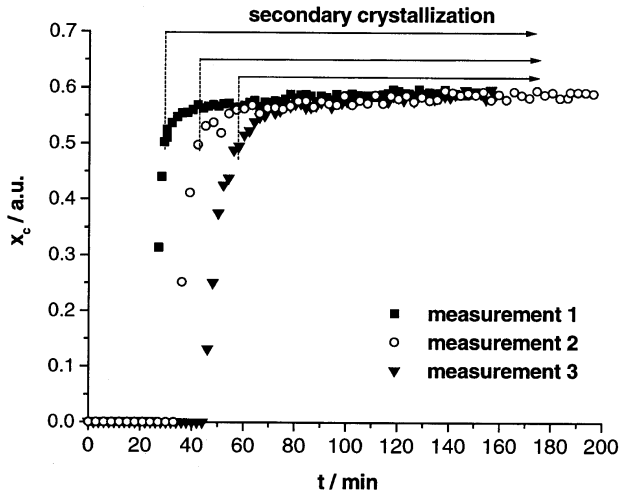


Fig. 7. Development of $x_c$ during the microfocus experiments for the isothermal crystallization of $PVF_2$ at 162°C. The vertical lines mark the time from which on secondary crystallization could be observed.

(outside of a spherulite). After the spherulite crossed the X-ray focus (approximately 30 min), reflections started to appear. In both cases, the crystallites exhibited a rotationally symmetric orientation distribution about the spherulite radius. The orientation of the crystallites did not change during the entire course of crystallization. The results of the microfocus experiments on iPP are represented in Fig. 6. The crystallinity, $x_c$, is shown as a function of time for the isothermal crystallization at 148°C (data acquisition started as soon as the sample had reached its crystallization temperature). For clarity, only three of the eight measurements are shown. In measurement 1, crystal reflections started to appear after 27 min because a spherulite crossed the area that was covered by the X-ray focus and a sudden increase of $x_c$ was observed. After another four minutes of growth, the spherulite had filled the irradiated volume completely and primary crystallization for that region was finished. At this point, the crystallinity was 48%. In the following time, all changes were due to secondary crystallization, i.e. further crystallization within the spherulite. It can be seen very clearly that the increase in $x_c$ was strongest just after the material was incorporated into the growing spherulite. After 260 min, $x_c$ approached a value of 61%. A slightly lower number was obtained by the conventional measurements. This can be explained with systematical errors inherent to the determination of $x_c$[3] [27,28].

Fig. 6 further shows that the spherulites were detected at different stages of primary crystallization. In measurement 1, a spherulite was detected in the very early stage of crystallization just after the induction period. For the measurements 2 and 3, the appearance of reflections was observed after 36 and 46 min of primary crystallization, respectively. In all eight experiments, reflections were first detected after 27 min and before 46 min of crystallization at $T_C$. Although secondary crystallization curves were observed in different spherulites and after different periods of annealing, all eight curves had practically the same shape indicating that the growth of secondary lamellae (or thickening of existing lamellae) was strongest just behind the growth front.

Although the spherulite was arbitrarily chosen, it is reasonable to assume that at eight random measurements the spherulites were observed in a variety of different growth states. It must, therefore, be concluded that secondary crystallization was strongest directly behind the growth front of the spherulite and was independent of its size or of the progress of its growth. Unfortunately, microcopy data could not be taken simultaneously to identify the growth state of the spherulite.

The curves of the microfocus measurements further showed that secondary crystallization did not account for only 10% of the overall crystallinity, as estimated from the conventional measurements, but for as much as 21%, if secondary crystallization effects during spherulite growth were considered as well. As shown by conventional measurements, the crystal lamellae developed during secondary crystallization have about the same size as those formed during primary crystallization indicating that relatively large amorphous regions must be present after primary crystallization.

Fig. 7 shows $x_c$ as a function of time for the isothermal crystallization of $PVF_2$ at 162°C. Three out of seven measurements are shown. In the case of $PVF_2$ the first growing spherulite could be observed after 20 min, corresponding to one third of the primary crystallization time. When the beam was completely within the spherulite, $x_c$ was 48%. During

[3] To determine the absolute value of $x_c$ of a semicrystalline polymer, it is necessary to measure X-ray scattering very high angles, which was impossible with the given set up.

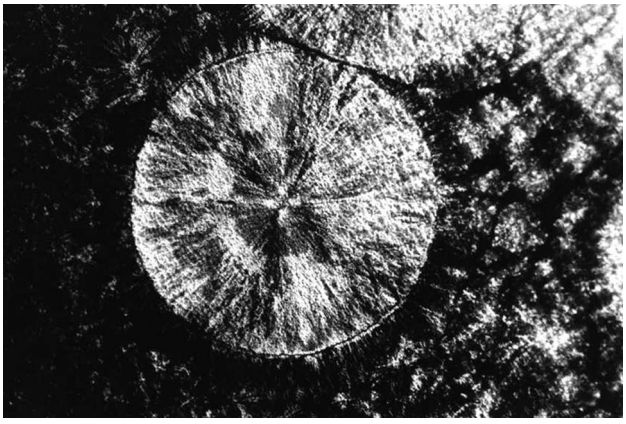

Fig. 8. Polarizing micrograph of a spherulite (200 μm in diameter) obtained by isothermal crystallization at $T_C = 152°C$ for 20 h. The spherulite of interest is surrounded by semicrystalline material forming much smaller spherulites of well below 10 μm in diameter.

the first 150 min of secondary crystallization, $x_c$ further increased to 62%. For the present conditions, secondary crystallization effects in $PVF_2$ accounted for 26% of the overall crystallization process, if the period of spherulite growth is considered as opposed to 13% as estimated from the conventional measurements.

In all seven experiments crystal reflections were detected within a time window of 17–44 min and followed the same growth kinetic. Measurement 3 of Fig. 7, however, represents a special case: the spherulite was detected after 44 min, thus, at the very end of primary crystallization as a comparison with Fig. 4 and Table 1 shows. It is, therefore, reasonable to assume that this spherulite had reached its final growth state just before it impinged onto other spherulites. Interestingly, even this curve was practically identical with the other six experiments, which represented earlier stages of primary crystallization. This finding is in very good agreement with the finding of Akpalu et al. who concluded that secondary crystallization effects predominate the late stage of spherulite growth.

The results for $PVF_2$ were very similar to those obtained on iPP. Secondary crystallization effects were strongest just after the amorphous material had been incorporated in the growing spherulite and the effects were strongest at the boundary of the spherulite, regardless of its growth state. This was true even if the spherulite was nearly fully grown just before it impinged onto other entities. Unfortunately, no $PFV_2$-spherulite could be observed short after the induction period, which would have provided secondary crystallization data over the whole period of spherulite growth.

### *3.4. Local variation of the crystallinity within a quenched spherulite*

To further study secondary crystallization effects inside growing superstructures, a spherulite was prepared under isothermal conditions and rapidly quenched before it impinged onto other spherulites. As a result of quenching, growth of new lamellae stacks and substantial lamellae thickening were frozen. Consequently, near the boundary secondary crystallization had progressed to a lesser degree than in the main body of the spherulite. Therefore, the radius of the spherulite corresponds to different stages of secondary crystallization inside the spherulite where the center represented a mature, and the boundary an initial stage of secondary crystallization.

Although thinner lamellae may have grown within existing lamellae stacks during quenching and storing at room temperature throughout the spherulite, this process would have occurred at the boundary as well as in the center. Therefore, it would not have changed the relative ratio of $x_c$ at the boundary and at the center. Unfortunately, the present set up did not allow to perform microfocus SAXS measurements to verify this.

Fig. 8 shows a polarizing micrograph of the resulting spherulite surrounded by semicrystalline material. The spherulite was obtained through isothermal crystallization at $T_C = 152°C$. After 20 h, the specimen was rapidly cooled to room temperature. Before quenching, the primary crystallization was not yet finished and a few large spherulites were situated in an amorphous matrix. These amorphous regions crystallized during quenching and formed much smaller spherulites having a diameter of well below 10 μm. Two-dimensional X-ray patterns of the spherulite were taken with the microfocus camera. It was scanned in steps of 10 μm from the center to the boundary.

Fig. 9 shows a comparison of the local variation of $x_c$ within the quenched spherulite and the development of $x_c$ from the beginning of secondary crystallization as obtained by the microfocus kinetic experiments. It can be seen that $x_c$ was lower at the boundary and nearly constant inside the quenched spherulite. The two curves have a very similar shape, which indicates that the variation of $x_c$ in the quenched spherulite was indeed due to different levels of secondary crystallization. The thickness of the boundary layer that had a lower $x_c$ was 30 μm, which corresponded to a radial growth period of 45 min.

At this point, it might be argued that fractionated crystallization according to Keith and Padden took place in the quenched spherulite that would have lead to the variation of $x_c$ along the radius of the spherulite [29,30]. Keith and Padden found that fast crystallizing material forms the inner part of the spherulite and slower crystallizing fractions and impurities are built in at a later state resulting in a lower crystallinity at the boundary of the spherulite. Calvert et al. concluded from ultra violet microscopy that secondary crystallization is not uniform within the spherulite but is strongly affected by the variations in the concentration of polymeric impurities rejected during the initial spherulite growth [31]. By contrast, the microscopy data reported in this paper showed a linear growth rate of the spherulite, which indicated that the concentration of the impurities

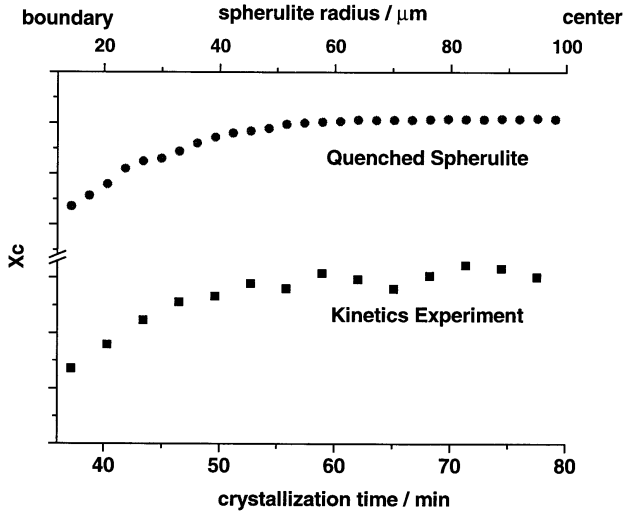


Fig. 9. Comparison of the progress of $x_c$ from the beginning of secondary crystallization as obtained from the μWAXS measurement of the crystallization kinetics and the local variation of $x_c$ within the quenched spherulite.

that might have existed, was constant at the growth front throughout the crystallization process. Hence, the impurities accumulate in the amorphous regions between bundles of crystalline lamellae. Moreover, the experiments on iPP and $PVF_2$ showed the same crystallization kinetics independent of the state of the growing spherulite. Therefore, it is concluded here that secondary crystallization is independent of the spherulite's growth state, but is closely coupled to the growth front. The local variation of $x_c$ found in the quenched iPP spherulite is due to different stages of secondary crystallization within that unit.

## 4. Conclusions

Secondary crystallization effects during spherulite growth were studied by using a combination of conventional simultaneous on-line WAXS/SAXS techniques and separate on-line microfocus measurement. The concept of the microfocus method allows studying the structural changes within the growing spherulite. Upon crystallization at low undercooling, iPP and $PVF_2$ form sufficiently large spherulites to successfully apply the microfocus technique. Conventional SAXS/WAXS measurements show that the main mechanism for secondary crystallization at low undercooling is the growth of new lamellae stacks into amorphous regions. No thinner crystals are inserted between lamellae within existing stacks because their melting point would have been lower than the crystallization temperature.

The microfocus measurement showed that an appreciable fraction of crystallites grow as a result of secondary crystallization (from a confined melt) while the spherulite was still growing. Furthermore, the contribution of secondary crystallization effects to the total crystallinity is underestimated when measured after the spherulite became volumen filling. Secondary crystallization effects were strongest closely behind the growth front of the spherulite and slowed down as the spherulite boundary moved away. This finding was confirmed by a separate off-line microfocus study of an isothermally crystallized and then quenched spherulite. The crystallinity varied locally within this spherulite; $x_c$ was lower near the boundary, where crystallization progressed to a lesser degree.

Since the kinetics of secondary crystallization did not depend on the actual growth state of the spherulite, it must be concluded that the concentration of impurities was constant at the boundary during the entire time of crystallization. The finding of a constant growth rate supports this. Moreover, in one instance, a very mature $PVF_2$-spherulite was detected just before the end of primary crystallization; its crystallization curve was practically identical to the ones found for spherulite formed during an earlier stage.

## Acknowledgements

The authors thank Ralph Doehrmann for excellent technical support. This research was carried out at the Hamburg Synchrotron Radiation Laboratory (HASYLAB) at DESY and at the European Synchrotron Radiation Facility (ESRF) and was partly founded by the German Federal Ministry of Science and Technology under the contract number 05-5 GUHXB.

## References

[1] Zachmann HG, Stuart HA. Makromol Chem 1960;49:131.
[2] Avrami MJ. J Chem Phys 1939;7:1103.
[3] Gordon M, Hillier IH. Trans Faraday Soc 1964;60:763.
[4] Peterlin A. J Appl Phys 1964;35:75.
[5] Perez-Cardenas FC, Castillo LF, Vera-Granziano R. J Appl Polym Sci 1991;43:779.
[6] Schultz JM, Scott RD. J Polym Sci, Part A-2 1969;7:659.
[7] Schultz JM, Fischer EW, Zachmann HG. J Polym Sci Polym Phys Edn 1980;18:239.
[8] Zachmann HG, Wuzt C. In: Doris M, editor. Crystallization of polymers. Dordrecht: Kluwer Academic Publushers, 1993. p. 403–14.
[9] Stein RS, Cronauer J, Zachmann HG. J Mol Struct 1996;383:19.
[10] Bark M, Zachmann HG, Alamo R, Mandelkern L. Macromol Chem 1992;193:2363.
[11] Bark M, Zachmann HG. Acta Polym 1993;44:259.
[12] Zachmann HG, Gehrke R. In: Sedlacek B, editor. Morphology of polymers. Berlin: Walter de Gruyte, 1986.
[13] Wang ZG, Hsiao BS, Sauer BB, Kampert WG. Polymer 1999;40:4615.
[14] Akpalu Y, Kilehorn L, Hsiao BS, Stein RS, Russell TP, van Egmond J, Muthukumar M. Macromolecules 1999;32:765.
[15] Gehrke R, Riekel C, Zachmann HG. Polymer 1989;30:1582.
[16] Ryan AJ, Stanford JL, Bras W, Nye TMW. Polymer 1997;38:759.
[17] O'Kane WJO, Young RJ, Ryan AJ, Bras W, Derbyshire GE, Mant GR. Polymer 1994;35:1352.
[18] Hsiao BS, Sauer BB, Verma RK, Zachmann HG, Seifert S, Chu B, Harney P. Macromolecules 1995;28:6931.

[19] Verma RK, Marand H, Hsiao B. Macromolecules 1996;29:7767.
[20] Engstrom P, Fiedler S, Riekel C. Rev Sci Instrum 1995;66(2):1348.
[21] Elsner G, Riekel C, Zachmann HG. Adv Polym Sci 1985;67:1.
[22] Schultz JM. J Polym Sci Polym Phys Edn 1976;14:2291.
[23] Kolb R. Submitted for publication.
[24] Marand H. Proceedings of American Chemical Society, vol. 81. New Orleans: American Chemical Society, 1999. p. 238.
[25] Schultz JM. Macromolecules 1996;29:3022.
[26] Krause TH, Kalinka G, Auer C, Hinrichsen G. J Appl Polym Sci 1994;51:399.
[27] Ruland W. Acta Crystallogr 1961;14:1180.
[28] Vonk CG. J Appl Crystallogr 1973;6:148–52.
[29] Keith HD, Padden Jr FJ. J Appl Phys 1964;35:1270.
[30] Keith HD, Padden Jr FJ. J Appl Phys 1964;35:1285.
[31] Calvert PD, Ryan TG. Polymer 1984;25:921.